Journal of Alloys and Compounds 900 (2022) 163386

Contents lists available at ScienceDirect

Journal of Alloys and Compounds

journal homepage: www.elsevier.com/locate/jalcom

Effect of ZnS coating on the optoelectronic properties of aqueous glutathione capped AgInS quantum dots

Nozikumbuzo Anati Vitshima, Bongiwe Silwana, Ncediwe Tsolekile*, Mangaka C. Matoetoe*

Department of Chemistry, Cape Peninsula University of Technology, P.O. Box 652, Cape Town 2000, South Africa

ARTICLE INFO

Article history:
Received 7 October 2021
Received in revised form 3 December 2021
Accepted 20 December 2021
Available online 24 December 2021

Keywords:
AgInS QDs
AgInS/ZnS QDs
Differential pulse voltammetry (DPV)
Cyclic voltammetry

ABSTRACT

Ternary I–III–VI quantum dots (QDs) have proved to be promising alternatives to the traditional binary Cd-QDs due to their inherently lower toxicities, greener synthetic methods, and tunable optoelectronic properties. Their application in the development of biosensors, electroluminescent devices, and a range of other electrochemical applications has resulted in the I–III–VI QDs receiving widespread attention in various fields. In this paper, water-soluble glutathione capped AgInS core QDs and AIS/ZnS core/shell QDs were synthesized using an eco-friendly hydrothermal method. Electrochemical properties of the AgInS core QDs and AgInS/ZnS core/shell QDs were evaluated using cyclic voltammetry (CV) and differential pulse voltammetry (DPV). DPV of AgInS core QDs exhibited distinguished oxidation peaks centred at − 0.05 and − 0.88 V vs Ag/AgCl of Ag and In ions, respectively, while the AgInS/ZnS QDs showed three symmetrically oxidation peaks at potentials − 0.87, − 0.66 and − 0.42 V of Zn, In and Ag ions, respectively. The total number of electrons, electron transport diffusion coefficient, De (in cm^2 s^1), and surface concentration of soluble species were evaluated and calculated using the Randles-Sevcik equation. The number of electrons was found to be 1.08 and 0.75 for AgInS QDs and AgInS/ZnS QDs, respectively using the Ag peak and the De value of AgInS QDs was greater than AgInS/ZnS QDs. This indicates that the electron diffusion was the slowest in the AgInS/ZnS QDs. The as-synthesized AgInS core QDs and AgInS/ZnS core-shell QDs exhibited chemical and electrochemical composition-dependent properties. This suggests the material is suitable for the development of biosensors.

1. Introduction

Ternary I–III–VI quantum dots (QDs) have been shown to possess superior optoelectronic properties, with tunable photoluminescence (PL) properties that are directly linked to their size, shape and composition [1,2]. The absence of toxic metals such as Cd, Pb or Hg has resulted in I–III–VI QDs receiving extensive attention amongst researchers. The high extinction coefficient, ability to serve as an efficient electron-conducting tunnel and tunable size of QDs has enabled their use in a variety of fields [3]. Intrinsically, the broad PL of ternary QDs has proved advantageous for the development of sensor systems, while the self-trapped exciton model of ternary QDs has been utilized in the construction of photovoltaics [4], [5]. Amongst several chalcopyrite QDs, the I–III-VI QDs (e.g., $CuInS_2$ and $AgInS_2$ QDs) are the most widely researched owing to their direct bandgap, large stokes shift, and long fluorescence lifetime [6].

The structure of QDs is composed of two distinct allied layers, namely the core and core/shell. The core of QDs is inherently the most reactive yet unstable layer that houses the optical properties of the QDs. Consequently, the core plays a central role in the fabrication and design of QDs. Overcoating of the core with a layer of another semiconductor material to form core/shell type QDs is one of the most widely used strategies to improve optical properties, control stability and enhance photoluminescence quantum yield (PLQY) of QDs [6], [7], [8]. Several materials (i.e., ZnS or CdS) have been employed as shelling materials. However, ZnS remains the most widely used passivating agent for its properties such as (i) high bandgap, (ii) low lattice mismatch and (iii) its low toxicity compared to other passivation materials [9], [6], [10]. Despite the rich amount of literature on the optical differences of the core and the core/shell structures of ternary QDs, there has been limited electrochemical investigations reported on the ternary I–III-VI QDs [11], [12], [13]. Moreover, as far as the authors know, there has been no report on the electrochemical differences in the properties of GSH capped AgInS core QDs and AgInS/ZnS core/shell QDs using cyclic voltammetry (CV) and differential pulse voltammetry (DPV).

* Corresponding authors.
E-mail addresses: tsolekilen@cput.ac.za (N. Tsolekile), matoetoem@cput.ac.za (M.C. Matoetoe).

https://doi.org/10.1016/j.jallcom.2021.163386
0925-8388/

In this study, glutathione capped AgInS core QDs and AgInS/ZnS core/shell QDs were synthesised using a simple one-pot green synthesis method. Temporal evolution of Ag: In ratio (1:1, 1:2, 1:4, 1:6, 1:8 and 1:16), reaction time (0, 15, 30, 45 and 60 min) and ZnS coating layers were investigated. Optimum conditions were obtained after 45 min synthesis time, Ag: In (1:4) molar ratio and one ZnS layer. The study of the electrochemistry of ternary QDs plays an important role in attaining information on the structural composition of QDs. Comparative study on the electrochemical properties of AgInS core QDs and AgInS/ZnS core/shell QDs was evaluated using cyclic voltammetry (CV) and differential pulse voltammetry (DPV). The results of this study showed that the as-synthesized AgInS QDs and AgInS/ZnS QDs exhibited chemical composition-dependent properties enabling the use of the materials in both electronics and biosensor applications.

2. Experimental

2.1. Materials

Silver nitrate ($AgNO_3$), Indium (III) chloride ($InCl_3$) tris-sodium citrate ($Na_3C_6H_5O_7$. 2 H_2O), L-Glutathione reduced (GSH), Sodium hydroxide (NaOH) pellets, Hydrochloric acid (HCl, 32%) and sodium sulphide (Na_2S), zinc acetate dihydrate ($Zn(O_2CCH_3)_2(H_2O)_2$), thiourea (CH_4N_2S) and ethanol (CH_3CH_2OH) were purchased from Sigma Aldrich, South Africa and used as received. Deionized water was used for the synthesis and analysis.

2.2. Synthesis of AgInS QDs and AgInS/ZnS QDs

Glutathione capped AgInS core QDs were synthesized according to the previously reported protocol with modifications [14]. In a typical synthesis, $AgNO_3$ (0.0107 g, 0.063 mmol), $InCl_3$ (0.055 g, 0.25 mmol), $Na_3C_6H_5O_7$ (0.294 g, 1.00 mmol), GSH (0.045 g, 0.145 mmol) were added to 100 mL of deionized water under magnetic stirring in a 250-mL three-neck flask. The pH was adjusted to 7.5 by the addition of small amounts of NaOH (1.0 M). Na_2S (0.0975 g/10 mL, 1.25 mmol) was then added under vigorous magnetic stirring and the resulting solution was refluxed at 95 °C for 45 min to form AgInS core QDs. After this period, $Zn(O_2CCH_3)_2(H_2O)_2$ (0.044 g/10 mL, 0.200 mmol) and CH_4N_2S (0.015 g/10 mL, 0.200 mmol) were added to the reaction mixture, which was then refluxed for 1 h 20 min at 95 °C to form AgInS/ZnS core/shell QDs. The experimental conditions for the synthesis of QDs were optimized by assessing the effect of reaction time, Ag: In molar ratio and the number of ZnS coatings required for the preparation of luminescent and water-soluble AgInS/ZnS core/shell QDs. For the precipitation of the obtained QDs, ethanol (200 mL) was added, and the dispersion was centrifuged. The precipitate was collected and redispersed in water, and the procedure was repeated two times. The obtained QDs samples were stored in amber glass vials at room temperature. Scheme. 1.

2.3. Characterization

The AgInS QDs and AgInS/ZnS QDs were characterized using; ultraviolet-visible spectrophotometry (UV–Vis) (Perkin Elmer UV–Vis Lambda 25 spectrometer, (UK); 1 nm slit width), photoluminescence (PL) (RF-6000, Shimadzu, Japan), fourier transform infrared spectroscopy (FT-IR) (Spectrum two UATR spectrometer, Perkin Elmer, UK), transmission electron microscopy (TEM). Electrochemical analysis was performed using Autolab PGSTAT 101 (Metrohm, South Africa). The photoluminescence quantum yield (PLQY) of AgInS core QDs and AgInS/ZnS core-shell QDs was calculated using rhodamine 6 G (QY = 0.95, ethanol solution) as a reference standard and the equation below:

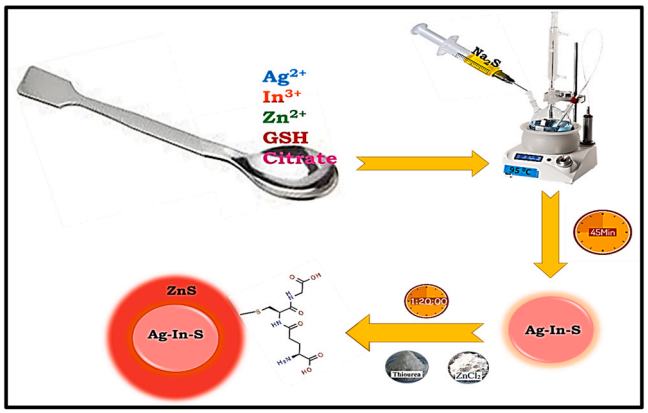

Scheme 1. Schematic illustration of the synthesis of water-soluble GSH capped AgInS QDs and AgInS/ZnS QDs.

$$QY\ (\%) = QY_R \times \frac{I \times A_R}{I_R \times A} \times 100$$

where QY_R is the quantum yield of the reference. I and I_R are the integrated intensities of the sample and standard, respectively. A and A_R are the absorbance of the sample and reference standard, respectively.

2.4. Electrochemical measurements

Electrochemical measurements were run using a typical conventional one-compartment three-electrode system connected to potentiostat Autolab PGSTAT 101 (Metrohm, SA) operating in software NOVA 2.1. The three electrodes used were glassy carbon (GC) as a working electrode, a platinum auxiliary electrode and Ag/AgCl reference electrode. The GCE was polished with alumina powder between the experiments to remove any residue deposits on the surface. Unless stated otherwise, all experiments were run using HCl (0.01 M) solution over a potential range − 1.5 to + 1.5 V. The synthetic metal quantum dots solution was dissolved in HCl (0.01 M) electrolyte solution. The HCl (0.01 M) solution was first analyzed to determine the background signal and the solution of AgInS QDs and AgInS/ZnS QDs were investigated. All electrochemical experiments were carried out in solutions purged with high purity nitrogen gas for 5 min

3. Results and discussion

AgInS core QDs was synthesised by mixing precursor cations (Ag^{2+} and In^{3+}) and anion (S^{2-}) species under strong magnetic stirring. Since Ag^+ is a soft Lewis acid and In^{3+} a hard acid, the reactivity of these metal ions needed to be well balanced and controlled during the reaction and This was achieved by employing a non-stoichiometric ratio of the metal ions (i.e. adding In^{3+} in four-fold excess), using two stabilizing agents (namely glutathione and sodium citrate as soft bases) and highly reactive Na_2S as a sulphur source [15]. In this study, GSH was selected as thiol capping for its biocompatible properties. Moreover, GSH is a tripeptide that contains different functional groups (i.e. amine and carboxylate groups) which can allow for further structural modifications. For optimum reaction conditions, three synthetic parameters (e.g. reaction time, Ag: In molar ratio, and different ZnS coating) were evaluated. Following successful synthesis and characterization of the AgInS core QDs, zinc acetate and thiourea were added as ZnS shell precursors to form AgInS/ZnS core/shell QDs.

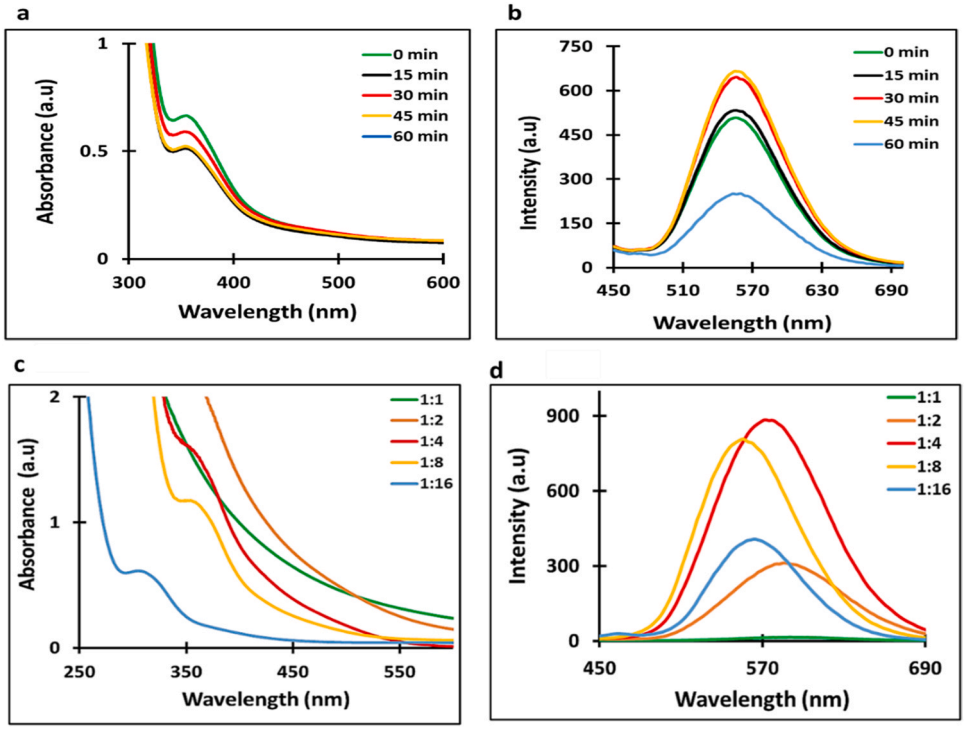

Fig. 1. Absorption spectra (a and c) and PL spectra (b and d) of AgInS core QDs at different reaction times and Ag: In molar ratios respectively.

3.1. Effect of synthesis reaction time

Fig. 1 shows the optical properties of AgInS core QDs measured using absorption (UV-Vis) and photoluminescence (PL) spectroscopy. The temporal evolution of the absorption spectra of AgInS QDs synthesized at 95 °C and analysed at different reaction times are shown in Fig. 1a.

The absorption spectra depict broad excitonic peaks centred around 359 nm. The absorptions decreased with increasing reaction time, with 0 min representing QDs aliquot at taken immediately after the addition of Na_2S as a sulfur source, signifying burst nucleation process. Moreover, the results Fig. 1b represents the corresponding PL of the synthesized AgInS QDs, as with the absorption spectra, broad PL emissions were obtained with emission wavelength centred around 559 nm. The PL intensity increased as a function of reaction time for 45 min after which a sharp decline in intensity was observed. The PL spectral wavelength remained relatively unaffected by synthesis time suggesting slow growth of QDs [16]. Based on the high PL intensity, 45 min was selected as the optimum reaction time for the synthesis of AgInS core QDs.

3.2. Ag:In ratio

The optical properties of ternary QDs are highly dependent on the amount of cation and can be tuned by varying the cation: anion ratio (viz Ag: In molar ratio in this study). Fig. 1c represents UV spectra of the as-synthesized QDs with nominal molar ratios varied from 1:1–1:16 (Ag: In). At ratio 1:1 and 1: 2, no distinct absorption peak was observed while molar.

ratios 1:4, 1:6, 1:8 and 1:16 exhibited broad excitonic peaks with increasing In content. The emission properties of the AgInS core QDs were highly dependent on the Ag: In molar ratio. The intensity of the QDs gradually shifted to higher intensities with increasing amounts of In with 1:4 (Ag: In) molar ratio exhibiting maximum intensities. The PL spectral position was tuned in a broad range from 558 to 582 nm, with ratio 1: 4 exhibiting the highest wavelength. Subsequently, molar ratio 1:4 (Ag: In) was selected as the optimum ratio in this study.

3.3. AgInS/ZnS core/shell QDs

To enhance the photophysical properties of the synthesized QDs, the ZnS shell was deposited on the AgInS core QDs. ZnS was selected as a passivation agent as it has a relatively low lattice mismatch of ~2.2% to ternary QDs and a wider bandgap (~3.7 eV). The effect of shell passivation was investigated by depositing three ZnS coatings over the AgInS core QDs. Fig. 2a shows the UV–vis absorption spectra with different ZnS coatings. The increase in the amount of ZnS added resulted in a blue shift in the onset of the AgInS/ZnS core QDs. As expected, deposition of ZnS over AgInS core QDs resulted in increased PL intensity compared to the AgInS core QDs which was accounted for the elimination of some defect states within the core and the subsequent overcoating of the core [20]. As the number of ZnScoatings increased, a continuous blue-shift from 582 nm (AgInS core) to 564, 541 and 525 nm for ZnS coating 1, 2 and 3, respectively was observed. The obtained blue-shift following ZnS passivation is a common phenomenon with ternary QDs and accounted as the diffusion of Zn^{2+} ions into the core via partial cationic (Ag^{+} or In^{3+}) exchange with the Zn^{2+} in the core [21], [14]. Based on the high intensity and maximum wavelength, AIS/ZnS core-shell QDs with one ZnS coating was used throughout this study. The PLQY of the AgInS core QDs was calculated to be 31.6% which increased to 35.4% for the AgInS/ZnS core/shell QDs. This confirms improvement in the quality of the material following ZnS passivation. Moreover, the luminescence and/ or QY of the as-synthesized QDs is seemingly superior to QDs synthesized using other ligands such as 1-dodecanethiol (DDT), thioglycolic acid (TGA) and mercapto propionic acid (MPA) [17], [18], [19].

The size and morphology of the synthesized QDs were examined using transmission electron microscopy (TEM). As depicted in Fig. 4a and c, the AgInS core QD and AgInS/ZnS core/shell QDs were small and spherical. The size of AgInS core QDs is centred around 1.5 nm while the AgInS/ZnS core/shell QDs exhibited particle size ~ 2.5 nm

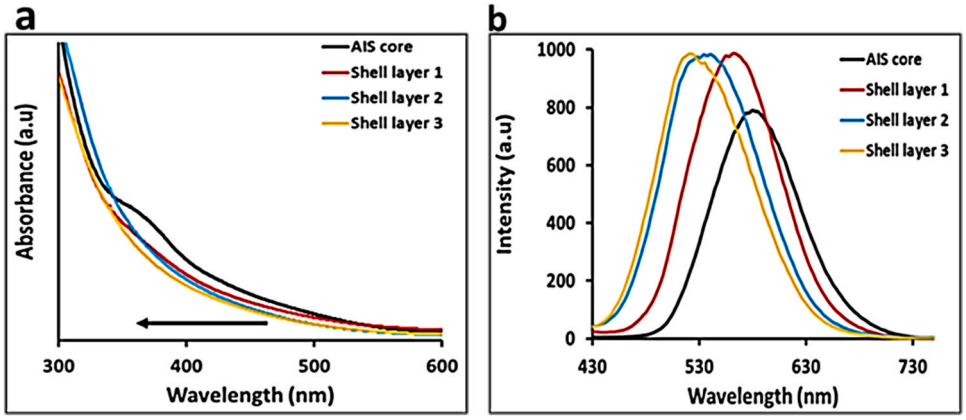

Fig. 2. Absorption spectra (a) and PL spectra (b) of AgInS/ZnS shell layers check the alphabets on the figures.

as shown in the size distribution curves (Fig. 4b, d). The hydrodynamic diameter (HD) and zeta potential of AgInS QDs and AgInS/ZnS QDs were measured using the dynamic light scattering (DLS) technique. As shown in S1 (Supplementary material), AgInS QDs exhibited narrow size distribution compared to AIS/ZnS core-shell QDs. As expected, the HD of the AgInS core QDs and AgInS/ZnS core-shell QDs was higher than sizes calculated using the TEM, this is in line with reported studies [22]. The zeta potential of the AgInS core QDs and AgInS/ZnS core/shell QDs was highly negative (−50 mV and −26 mV respectively) indicating the high degree of colloidal stability of the synthesized material.

FTIR spectra were evaluated to confirm GSH capping on the surface of the as-synthesized AgInS QDs and AgInS/ZnS QDs as shown in Fig. 3. The FTIR spectrum of GSH exhibited sharp bands at 3340 cm^{-1} and 3251 cm^{-1} which were attributed to vOH and -NH functional groups, respectively. AgInS core QDs exhibited a shift and peak broadening of the vOH and vC-H functional groups. The disappearance of the GSH thiol (vS-H) peak in the AgInS QDs spectrum indicates vS-H group was involved in the passivation of the AgInS core QDs surface with GSH. Following ZnS passivation, the AgInS/ZnS QDs exhibited similar spectra of the GSH capped core but with a slight reduction in intensity and peak shift in the vO-H and vC-H bands. Furthermore, the AgInS/ZnS QDs exhibited vC=O at 1560 cm^{-1}(asymmetrical) and 1358 cm^{-1} (symmetrical) confirming capping of as-synthesized AgInS/ZnS QDs with glutathione.

3.4. Electrochemical characterization of AgInS core QDs and AgInS/ZnS core/shell QDs

Fig. 5 shows comparative cyclic voltammograms (CV) and differential pulse voltammograms (DPV) at the glassy carbon electrode

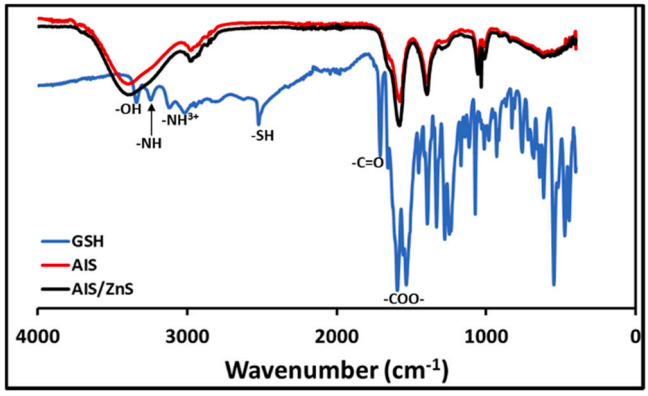

Fig. 3. FTIR spectra of GSH, AgInS core QDs and AgInS/ZnS core/shell QDs.

(GCE) in 0.01 M HCl solution of AgInS QDs and AgInS/ZnS QDs at a scan rate of 0.1 V /s. There was no observed response at the GCE in 0.01 M HCl in both CV and DPV in the absence of the QDs. By comparing the electrochemical behaviour of AgInS QDs and AgInS/ZnS QDs, a pair of weak redox peaks was observed in a CV of AgInS QDs at (Epa) = 0.14 V and Epc = −0.27 V with a formal potential of − 0.065 V vs Ag/AgCl. The oxidation peak at 0.14 V was attributed to Ag^+ ions generated from AgInS QDs and the reduction peak at − 0.27 V was associated with the reduction of Ag^+ to Ag^0. This observation has been reported previously with similar behaviour [23], [24], [25]. An interesting observation was made in the CV of the AgInS/ZnS QDs for the appearance of a small cathodic peak at (Epc) = −1.10 V vs Ag/AgCl and two sets of redox signals which appeared at (Epa) = 0.24 and 0.75 V and (Epc) = −0.21 and − 0.76 V corresponds to the following reactions:

$$Ag^0 \rightarrow Ag^+ + e \quad (1)$$

$$Ag + e \rightarrow Ag^0 \quad (2)$$

$$In^0 \rightarrow In^{3+} + 3e \quad (3)$$

$$In^{3+} + 3e \rightarrow In^0 \quad (4)$$

Indium redox peaks on a bare GCE has been reported at − 0.8 and − 0.57 V vs Ag/AgCl [26]. Further investigations were also conducted in the quest for a possible electrochemical characterization of AgInS QDs core and AgInS/ZnS QDs core-shell (Fig. 5b). For this, DPV was used as a fast, effective, and more sensitive electrochemical technique compared to CV [27]. As illustrated in Fig. 5b, DPV of AgInS QDs core exhibited distinguished oxidation peaks centred at − 0.05 and − 0.88 V vs Ag/AgCl of Ag and In ions, respectively, while the AgInS/ZnS QDs shows three symmetrically oxidation peaks at potentials − 0.87, − 0.66 and − 0.42 V of Zn, In and Ag ions, respectively. The CV data are in agreement with the DPV data. However, the current response of AgInS/ZnS QDs in the case of CV is greater than that of DPV. This may be because of the efficient elimination of capacitance current.

The total number of electrons, electron transport diffusion coefficient, De (in cm^2 s^1), and surface concentration of soluble species which react on the electrode surface with the formation of insoluble product, can be calculated according to Randles-Sevcik equation: (Eq. 1) [28].

$$Ip = 2.69 \times 10^5 n^{2/3} \times A \times D_{OX}^{1/2} \times C_{OX}^{*} \times V^{1/2} \quad (5)$$

where Ip is peak current, n is the total number of electrons transferred, A is the area of the working, 0.0707 cm^2, C is the concentration. Based on these results, the number of electrons was found to be 1.08 and 0.75 for AgInS QDs and AgInS/ZnS QDs, respectively using the Ag peak. This shows that both AgInS QDs and

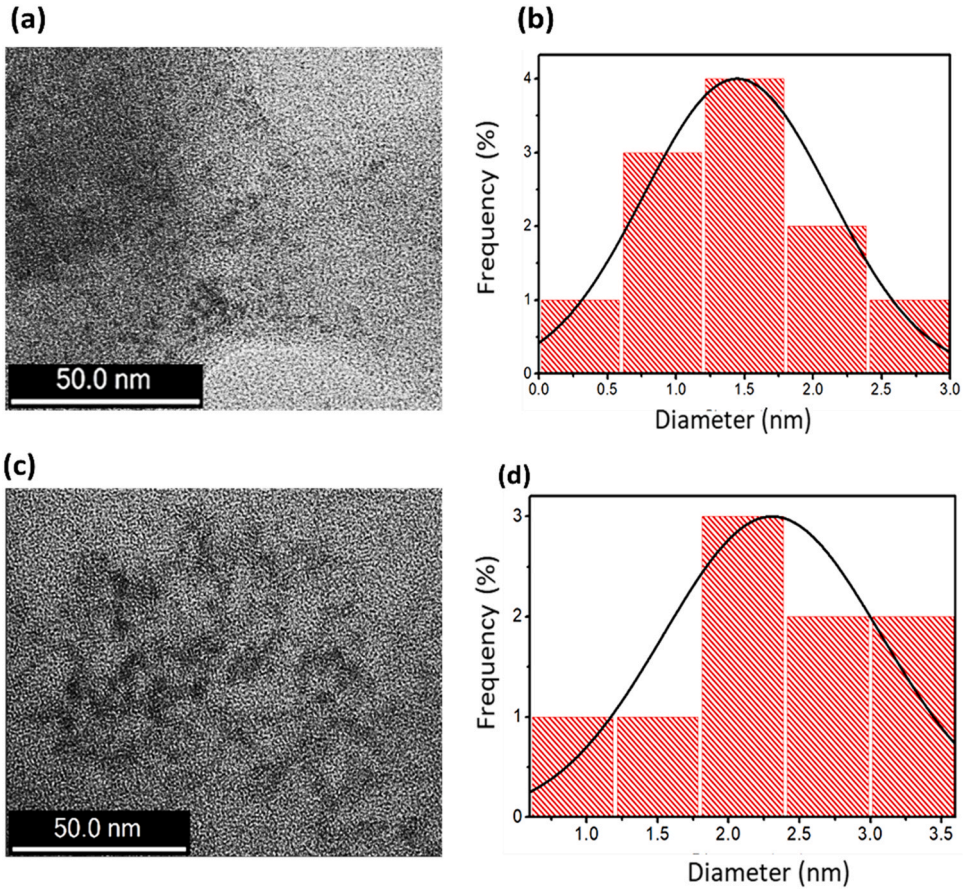

Fig. 4. (a) TEM and (b) particle size distribution of AgInS core QDs. (c) TEM and (d) particle size distribution of AgInS/ZnS core/shell QDs.

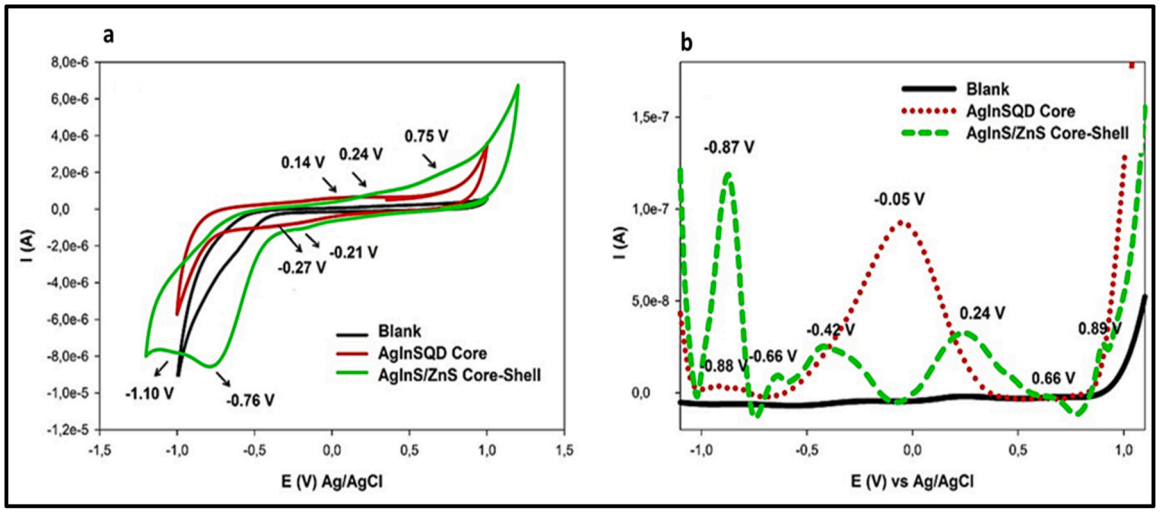

Fig. 5. CVs a) and DPVs b) obtained at GCE, blank, AgInS core QD, and AgInS/ZnS Core-Shell QD in 0.01 M HCl at scan rate 0.1 V/s.

AgInS/ZnS QDs undergo a one-electron reaction at the GCE in 0.01 M HCl. The value of De was found to be in the order AgInS QDs > AgInS/ZnS QDs. This indicates that the electron diffusion was the slowest in the AgInS/ZnS QDs. The surface concentration of the AgInS QDs and AgInS/ZnS QDs on a GCE was also calculated, by applying Eq. 6 [29], [30] and using the slope for the plot of Ip vs square root scan rate.

$$Slope = \frac{n^2.\ F^2.\ A.\ \Gamma}{4RT} \quad (6)$$

where Ip is the peak current at a given scan rate ν, n is the number of electrons transferred, F is the Faraday constant and A is the geometric area of the electrode. The electroactive surface concentration of AgInS QDs was greater than that of AgInS/ZnS QDs.

GCE	E^0 (V)	n	De ($cm^2\ s^1$)	Γ ($mol.\ cm^{-1}$)
AgInS QDs	-0.065	1.08	1.33×10^{-18}	3.18×10^{-6}
AgInS/ZnS QDs	0.015	0.75	8.11×10^{-20}	9.42×10^{-7}

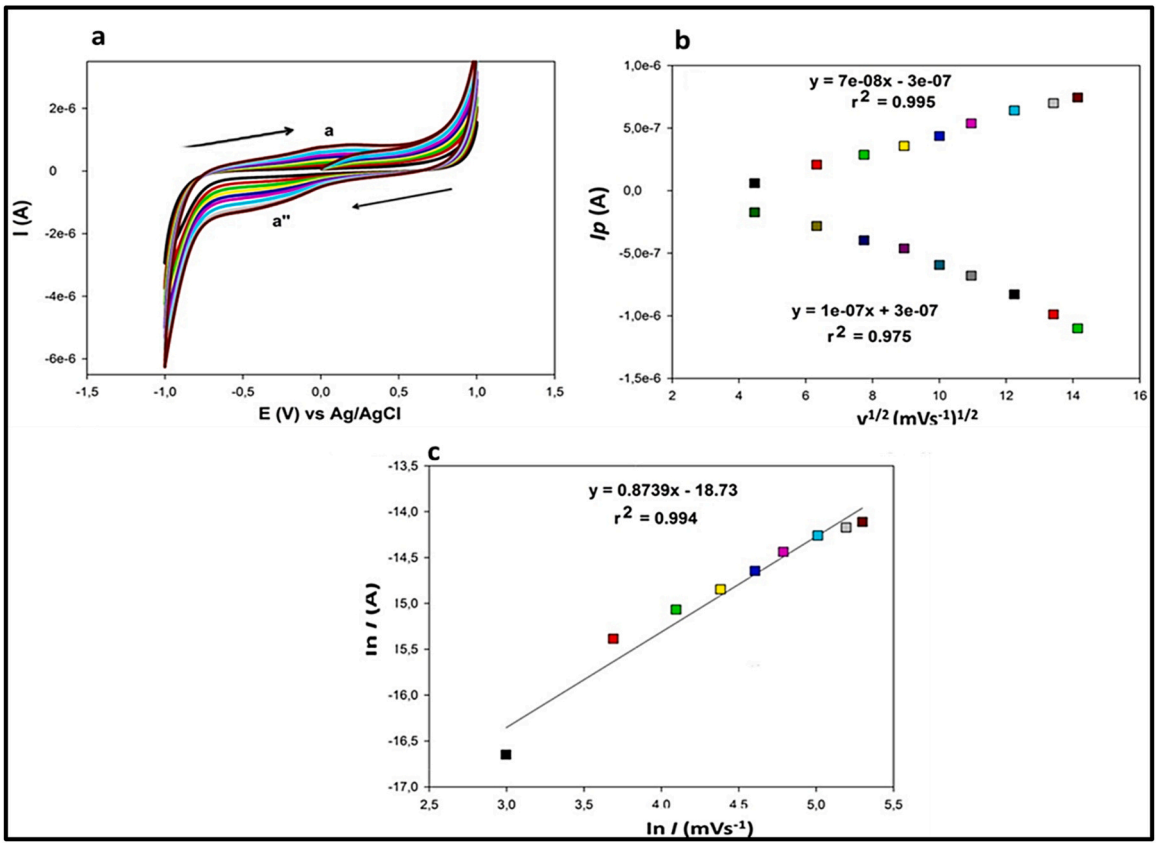

Fig. 6. Cyclic voltammetry for the effect of variation of scan rates (20 mV/s to 200 mV/s) of AgInS QDs from − 1.0–1.0 V/s on a GCE in 0.01 M HCl, a) Graph of the dependence of the anodic and cathodic peak current with square root scan rate b) Graph of In anodic peak current vs In scan rate c).

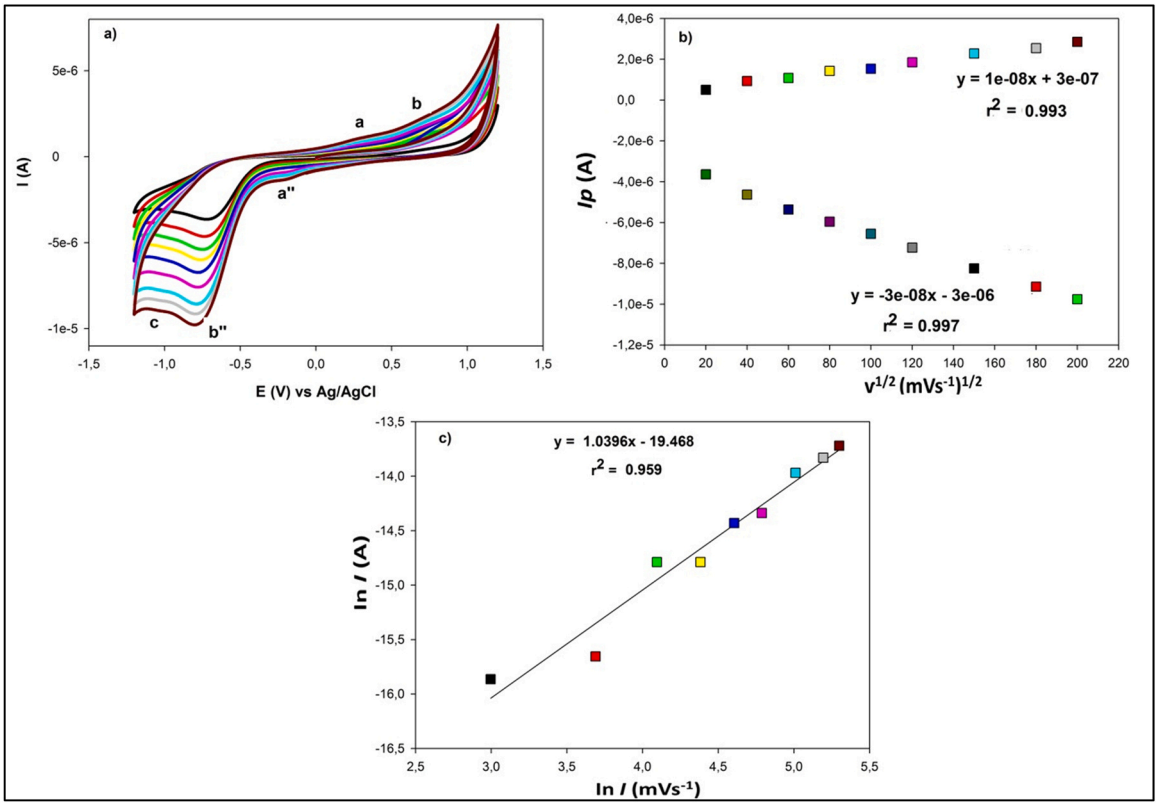

Fig. 7. Cyclic voltammetry for the effect of variation of scan rates (20 mV/s to 200 mV/s) of AgInS/ZnS from 1.0 V to 1.0 V/s on a GCE in 0.01 M HCl, a) graph of the dependence of the anodic and cathodic peak current with square root scan rate b) graph of In anodic peak current vs In scan rate c).

Furthermore, the variation of the scan rates (10 mV/s to the highest scan rate of 200 mV/s) was studied to evaluate the rate-limiting step on AgInS QDs core and AgInS/ZnS core-shell QDs and this is shown in Figs. 6 and 7. Two ways widely employed to study the reversibility of a reaction and to assess whether a reaction is adsorption or diffusion consist of the dependencies: Ip vs $v^{1/2}$ and In Ip vs In v [28], [31].

The Randles-Sevcik equation suggests that the linear relationship occurs between the peak current (Ip) of a freely diffusing reversible electrochemical redox species and the square root of its scan rate. Deviation from this relationship could mean quasi-reversible or surface adsorption. In Fig. 6 the peak current (Ipa) increases linearly with the square root of the scan rate while the peak current (Ipc) increases linearly with the square root for the scan rate less than 0.1 V/s (Fig. 6b). At scan rate greater than 0.1 V/s data deviates exhibiting values lower than those expected, a feature typically observed when an electrochemical reaction involves a nucleation step [32]. Following the Randles-Sevcik equation suggestion, the dependence of Ip vs square root scan rate plots deviates exhibiting values lower than those expected which is the characteristic of a quasi-reversible and adsorption control system. On the other hand, In Ip vs Inv gave a slope of 0.8739 close to 1, which is the indication of an adsorption-controlled system. A slope equal to 1 or close to one is expected for the adsorption process.

Fig. 7 shows the influence of the scan rate of the AgInS/ZnS core-shell. The values of oxidation and reduction peak current plotted against square root scan rates were both linear but does not pass through the origin which is the characteristic of quasi-reversible and adsorption control system. In Ip vs Inv a slope of 1.0386 was obtained, which is the indication of an adsorption-controlled system.

The optical and electrochemical results obtained in this study confirm the potential of the synthesised material in the electro-biochemical application. This is consistent with reported studies whereby ternary QDs have been synthesized for electrochemical biosensors [33], solar cells [34] and bio-applications [35].

4. Conclusions

This study was aimed to provide a better understanding of the optical and electrochemical variances of the AgInS core QDs and AgInS/ZnS core/shell QDs. Optimal conditions of the optical properties of the AgInS core QDs were obtained after 45 min synthesis at Ag: In molar ratio of 1:4. The addition of multiple ZnS shell monolayers for the formation of AgInS/ZnS core-shell QDs resulted in a blue shift in PL peak position. Both AgInS QDs and AgInS/ZnS QDs are adsorption controlled, with the Ag^+ showing a one-electron system. Higher currents were observed for the core strongly suggesting higher conductivity and electrical properties. These are further confirmed by fact that the core had a large electroactive surface. Comparative study of the electrochemical properties of AgInS QDs and AgInS/ZnS QDs showed that the as-synthesized AgInS QDs and AgInS/ZnS QDs exhibited chemical and electrochemical composition-dependent properties enabling the use of the materials in both electronics and bio-applications.

Declaration of Competing Interest

The authors declare that they have no known competing financial interests or personal relationships that could have appeared to influence the work reported in this paper.

Acknowledgements

The authors would like to thank the National Research Foundation (NRF), South Africa under the Thuthuka Grant (Grant No: 121986), Cape Peninsula University of Technology, South Africa.

Appendix A. Supporting information

Supplementary data associated with this article can be found in the online version at doi:10.1016/j.jallcom.2021.163386.

References

[1] A.M. Wagner, J.M. Knipe, G. Orive, N.A. Peppas, Quantum dots in biomedical applications, Acta Biomater. 94 (2019) 44–63.
[2] J. Wang, T. Deng, D. Deng, R. Zhang, Y. Gu, X. Zha, Quaternary alloy quantum dots with widely tunable emission–a versatile system to fabricate dual-emission nanocomposites for bio-imaging, RSC Adv. 6 (2016) 53760–53767.
[3] L. Chang, X. He, L. Chen, Y. Zhang, A novel fluorescent turn-on biosensor based on QDs@GSH–GO fluorescence resonance energy transfer for sensitive glutathione S-transferase sensing and cellular imaging, Nanoscale 9 (2017) 3881–3888.
[4] J.X. Soares, K.D. Wegner, D.S. Ribeiro, A. Melo, I. Häusler, J.L. Santos, U. Resch-Genger, Rationally designed synthesis of bright AgInS 2/ZnS quantum dots with emission control. Nano, Research 13 (2020) 2438–2450.
[5] X. An, Y. Zhang, J. Wang, D. Kong, X. He, L. Chen, Y. Zhang, The Preparation of $CuInS_2$-ZnS-Glutathione Quantum Dots and Their Application on the Sensitive Determination of Cytochrome c and Imaging of HeLa Cells, ACS Omega 6 (2021) 17501–17509.
[6] N. Tsolekile, S. Parani, M.C. Matoetoe, S.P. Songca, O.S. Oluwafemi, Evolution of ternary I–III–VI QDs: Synthesis, characterization, and application, Nanostruct. Nano-Objects 12 (2017) 46–56.
[7] Y. Ding, H. Sun, D. Liu, F. Liu, D. Wang, Q. Jiang, Water-soluble, high-quality ZnSe@ ZnS core/shell structure nanocrystals, J. Chin. Adv. Mater. Soc. 1 (2013) 56–64.
[8] Y. Chen, S. Li, L. Huang, D. Pan, Low-cost and gram-scale synthesis of water-soluble Cu–In–S/ZnS core/shell quantum dots in an electric pressure cooker, Nanoscale 6 (2014) 1295.
[9] L. Changa, X. Hea, L. Chena, Y. Zhanga, Mercaptophenylboronic acid-capped Mn-doped ZnS quantum dots forhighly selective and sensitive fluorescence detection of glycoproteins, Sens. Actuators B 243 (2017) 72–77.
[10] T. Jiang, J. Song, H. Wang, X. Ye, H. Wang, W. Zhang, M. Yang, R. Xia, L. Zhu, X. Xu, Aqueous synthesis of color tunable Cu doped Zn–In–S/ZnS nanoparticles in the whole visible region for cellular imaging, J. Mater. Chem. B 3 (2015) 2402–2410.
[11] O. Stroyuk, O. Raievska, C. Kupfer, D. Solonenko, A. Osvet, M. Batentschuk, C.J. Brabec, D.R.T. Zahn, High-Throughput Time-Resolved Photoluminescence Study of Composition- and Size-Selected Aqueous Ag–In–S Quantum Dots, J. Phys. Chem. C. 125 (2021) 12185–12197.
[12] I.A. Mir, M.A. Bhat, Z. Muhammad, S.U. Rehman, M. Hafeez, Q. Khan, L. Zhu, Differential and comparative sensing modes of AIS and AIS@ZnS core-shell quantum dots towards bioanalytes, J. Alloy. Compd. 811 (2019) 151688.
[13] K. Ghanbaria, M. Roushania, E. Soheylib, R. Sahraei, An electrochemical tyrosinamide aptasensor using a glassy carbon electrode modified by N-acetyl-L-cysteine-capped Ag-In-S QDs, Mater. Sci. Eng. C 102 (2019) 653–660.
[14] N. Tsolekile, S. Nahle, N. Zikalala, S. Parani, E.H.M. Sakho, O. Joubert, M.C. Matoetoe, S.P. Songca, O.S. Oluwafemi, Cytotoxicity, fluorescence tagging and gene-expression study of CuInS/ZnS QDS – meso (hydroxyphenyl) porphyrin conjugate against human monocytic leukemia cells, Sci. Rep. 10 (2020) 4936.
[15] Y. Chen, S. Li, L. Huang, D. Pan, Green and Facile Synthesis of Water-Soluble Cu–In–S/ZnS Core/Shell Quantum Dots, Inorg. Chem. 52 (2013) 7819–7821.
[16] S. Chen, M. Ahmadiantehrani, N.G. Publicover, K.W. Hunter, X. Zhu, Thermal decomposition-based synthesis of Ag-In-S/ZnS quantum dots and their chlorotoxin-modified micelles for brain tumor cell targeting, RSC Adv. 5 (2015) 60612–60620.
[17] M. Miropoltsev, V. Kuznetsova, A. Tkach, S. Cherevkov, A. Sokolova, V. Osipova, Y. Gromova, M. Baranov, A. Fedorov, Y. Gun'ko, A. Baranov, FRET-Based Analysis of $AgInS_2$/ZnAgInS/ZnS Quantum Dot Recombination Dynamics, Nanomaterials 10 (2020) 2455.
[18] B.M.M. May, S. Parani, O.S. Oluwafemi, Detection of ascorbic acid using green synthesized $AgInS_2$ quantum dots, Mater. Lett. 236 (2019) 432–435.
[19] H. Shi, L. Jia, C. Wang, E. Liu, Z. Ji, J. Fan, A high sensitive and selective fluorescent probe for dopamine detection based on water soluble $AgInS_2$ quantum dots, Opt. Mater. 99 (2020) 109549–109557.
[20] S. Mei, J. Zhu, W. Yang, X. Wei, W. Zhang, Q. Chen, L. He, Y. Jiang, R. Guo, Tunable emission and morphology control of the Cu-In-S/ZnS quantum dots with dual stabilizer via microwave-assisted aqueous synthesis, J. Alloy. Compd. 729 (2017) 1–8.
[21] T. Chen, X. Hu, Y. Xu, L. Wang, W. Jiang, Z. Xie, Hydrothermal synthesis of highly fluorescent Ag–In–S/ZnS core/shell quantum dots for white light-emitting diodes, J. Alloy. Compd. 804 (2019) 119–127.

[22] C. Chen, D. Wu, Y. Chan, C.C. Lin, P. Chung, M. Hsiao, R. Liu, Evaluations of the Chemical Stability and Cytotoxicity of $CuInS_2$ and $CuInS_2$/ZnS Core/Shell Quantum Dots, Green. Chem. 22 (2020) 1239–1248.
[23] F.O. Okumu, B. Silwana, M.C. Matoetoe, Application of MWCNTs/Ag-Pt nanocomposite modified GCE for the detection of Nevirapine in Pharmaceutical Formulation and Biological samples, Electroanalysis 32 (2020) 3000–3008.
[24] C. Van der Horst, B. Silwana, E. Iwuoha, V. Somerset, Synthesis and Characterization of Bismuth-Silver Nanoparticles for Electrochemical Sensor Applications, Anal. Lett. 48 (2015) 1311–1332.
[25] C. Yong-Jae, T.M. Luo, Electrochemical Properties of Silver Nanoparticle Doped Aminosilica Nanocomposite, Int. J. Electrochem., Hindawi 2011 (2011) 1–6, https://doi.org/10.4061/2011/404937
[26] A.M.K. Gustafsson, F. Bjorefors, B.-M. Steenari, C. Ekberg, Investigation of an electrochemical method for separation of copper, indium and galliumfrom pretreated CIGS Solar Cell Waste Material, Sci. World J. (2015) 494015.
[27] G. Wang, G. Shi, X. Chen, R. Yao, F. Chen, A glassy carbon electrode modified with graphene quantum dots and silver nanoparticles for simultaneous determination of guanine and adenine, Microchim. Acta 182 (2015) 315–322.
[28] P.T. Kissinger, W.R. Heineman, Laboratory Techniques in Electroanalytical Chemistry, Marcel Dekker, Inc, New York, USA, 1996.
[29] R.O. Akinyeye, I. Michira, M. Sekota, A.A. Ahmed Tito, D. Baker P.G.L., C.M.A. Brett, M. Kalaji, E. Iwuohaa, Electrochemical Synthesis and Characterization of 1,2-Naphthaquinone-4-Sulfonic Acid Doped Polypyrrole, Electroanalysis 19 (2007) 303–309.
[30] A.P. Brown, F.C. Anson, Anal. Chem. 49 (1977) 1589.
[31] A.J. Bard, L.R. Faulkner, Electrochemical, Methods: Fundamentals and Applications, 2nd edition., John Wiley & Sons, New York, 2001.
[32] D.J. Hills, S.J. Thompson, Electrochemical nucleation from molten salts—I. Diffusion controlled electrodeposition of silver from alkali molten nitrates, Electrochim. Acta19 (1974) 657–670.
[33] C. Li, J. Hu, M. Lu, C. Zhang, Quantum dot-based electrochemical biosensor for stripping voltametric detection of telomerase at the single-cell level, Biosens. Bioelectron. 122 (2018) 51–57.
[34] Z. Xiao, Y. Li, B. Yao, Z. Ding, R. Deng, H. Zhao, L. Zhang, Z. Zhang, Significantly enhancing the stability of a Cu_2ZnSnS_4 aqueous/ethanol-based precursor solution and its application in $Cu_2ZnSn(S,Se)_4$ solar cells, RSC Adv. 5 (2015) 103451.
[35] C.R. Hurtado, G.R. Hurtado, G.L. Cena, R.C. Queiroz, A.V. Silva, M.F. Diniz, V.R. Santos, V. Trava-Airoldi, M.S. Baptista, N. Tsolekile, O.S. Oluwafemi, K. Conceição, D.B. Tada, Diamond Nanoparticles-Porphyrin mTHPP Conjugate as photosensitizing Platform: Cytotoxicity and Antibacterial Activity, Nanomaterials 11 (2021) 1393.